Flexible Silicon-based Hydrogen-Bonded Organic Framework for Quasi-Solid-State Lithium Metal Batteries

Xin-Ying Huang[a†], Mao-Lin Guo[b†], Shang-Qi Li[b], Ji-Wei Liu[a], Yingnan Cao[*c], Chaofei Guo[*a]

1. Experimental Section

1.1 *Materials:*

Tetrakis(4-bromophenyl)silane (TBPSi, 650 mg, 1 mmol) was purchased from Jilin Chinese Academy of Sciences Yanshen Technology. Potassium carbonate (K_2CO_3, AR, ≥ 99.0%), 1,4-dioxane (AR, ≥ 99.5%), dichloromethane (CH_2Cl_2, AR, ≥ 99.5%), $MgSO_4$ (≥ 97.0%), ethyl acetate (AR, ≥ 99.5%) were purchased from sinopharm.

1.2 *Synthesis of TPPSi:*

Under Ar atmosphere, tetrakis(4-bromophenyl)silane (TBPSi, 650 mg, 1 mmol), $Pd(PPh_3)_4$ (700 mg, 0.06 mmol), 1-(tetrahydro-2H-pyran-2-yl)-4-(4,4,5,5-tetramethyl-1,3, 2-dioxaborane-2-yl)-1H-pyrazole (1.26 g, 4.5 mmol) and Potassium carbonate (K_2CO_3, 2.21 g, 16 mmol) were added to a mixed solvent of 1,4-dioxane and deionized water. The mixture was stirred at 95 °C for 72 h. Then, the mixture was cooled to room temperature, and 1,4-dioxane was removed under reduced pressure. The obtained residue was extracted with dichloromethane. The organic phase was dried over anhydrous $MgSO_4$, filtered, and the solvent was evaporated to afford the product. The product was purified by column chromatography (eluent: dichloromethane/ethyl acetate = 2:1). Subsequently, the resulting THP-protected intermediate was dissolved in a mixture of concentrated hydrochloric acid and methanol and stirred at 60 °C for 12 h to deprotect the compound. After, the solution was poured into distilled water, and the pH was adjusted to 9-10 using K_2CO_3. The precipitate was filtered off, washed with water, and dried at 80 °C to yield the white solid TPPSi.

1.3 *Preparation of Si-HOF:*

Dissolve 100 mg of TPPSi in DMSO and heat until the solution becomes

transparent， then allow the solution to stand at room temperature for 3 days. The milky-white Si-HOF solid was isolated by filtration. Finally, the resulting product was activated in a vacuum oven at 80 °C for 24 h.

1.4 ***Preparation of Si-HOF SSEs membrane:***

200 mg of Si-HOF, 50 mg of PVDF-HFP, and 30 mg of LiTFSI were dispersed in 1 mL of CH_3CN and treated under vigorous stirring for 12 h to obtain a uniformly dispersed slurry. Subsequently, the resulting mixture was coated onto a glass substrate and dried under vacuum at 80 °C for 12 h to form a membrane. The membrane was then immersed in a 1 M LiTFSI/PC solution for 12 h to undergo activation treatment. Finally, the resulting Si-HOF-based solid-state electrolytes (Si-HOF-based SSEs) was vacuum-dried in a cleanroom environment. For comparison, a solid-state electrolyte membrane without Si-HOF (SSEs without Si-HOF) was also prepared using the same procedure as above, except that Si-HOF was not added.

1.5 ***Materials characterizations:***

X-ray diffraction (XRD) analysis was performed on a Bruker D8 ADVANCE diffractometer; The specific surface area and pore size distribution were determined using a Micromeritics ASAP 2460 analyzer. Fourier-transform infrared (FT-IR) spectra were recorded on a Nicolet iS50 spectrometer. X-ray photoelectron spectroscopy (XPS) was conducted on Kratos AXIS SUPRA spectrometer. time-of-flight secondary ion mass spectrometry (TOF-SIMS) was performed on ION TOF-SIMS 5; Thermal Gravimetric (TG) was tested on HITACHI STA200/HITACHI STA300.

1.6 ***Electrochemical tests:***

Ionic conductivity: Ionic conductivity (σ) of the electrolyte was measured via EIS operated with two stainless steel (15.8 mm × 15.8 mm) electrodes symmetrically placed onto Si-HOF SSEs (thickness: 60 μm, diameter: 16 mm). The electrochemical impedance spectroscopy (EIS) was collected using an electrochemical working station at open circuit potential with constant perturbation amplitude of 10 mV in the frequency of 1 Hz-100 KHz. The Li^+ conductivity is calculated according to equation:

$\sigma = L/(R\ A)$, L = 60 μm， A=1.9606 cm^2

where σ is the Li^+ conductivity, S cm^{-1}; l is the thickness of the separator, cm, R_b is the bulk resistance, Ω; R_b can be obtained by the X-intercept, which is not directly correlated with the slope of the impedance plot. And A is contact area, cm^2.

$$\sigma = \frac{L}{R \times S} \quad (1)$$

Electrochemical window tests were performed on Li|SSE|SS cells using a CHI 660E electrochemical workstation, with a scan rate of 10 mV s^{-1} and a linear sweep voltammetry (LSV) scan from open-circuit voltage to 6 V. By combining AC impedance measurements with constant-potential polarization measurements, the Li^+ transfer number (t_{Li+}) of the Li|SSEs|Li symmetric cell was calculated using Equation (2) (1×10^5 Hz - 0.1 Hz, $\Delta V$is the direct current (DC) polarization voltage (10 mV), I_0 and I_s are the initial and stable currents during polarization, and R_0 and R_s are the impedances before and after polarization1).

$$t_{Li+} = \frac{I_S(\Delta V - I_0 R_0)}{I_0(\Delta V - I_S R_S)} \quad (2)$$

Measurements of Li|Li asymmetric cells were implemented at Neware testing system from 0.1 to 3 mA cm^{-2}. For full cells, the cathode was prepared by mixing 80 wt% $LiFePO_4$ (or $LiNi_{0.8}Co_{0.1}Mn_{0.1}O_2$) 10 wt% carbon black, and 10 wt% PVDF in NMP. It was then coated onto Al foil and dried in a vacuum oven at 120 °C for 12 h. The Li|SSE|LFP cells were assembled in CR2032 coin cells within an Ar-filled glove box, using LFP cathodes with an areal loading of 2.0 mg cm^{-2}. The anode electrode is lithium metal, the separator is Si-HOF-based SSEs or SSEs without Si-HOF, and no additional electrolyte is added. The cells were tested over a voltage window of 2.4 - 4.0 V at various current densities (1 C = 170 mA g^{-1}) on a Neware battery testing system. For comparison, Li|SSE|NCM_{811} ($LiNi_{0.8}Co_{0.1}Mn_{0.1}O_2$, NCM_{811}) cells were also fabricated under identical conditions, employing NCM_{811} cathodes with a similar areal loading (2.0 mg cm^{-2}) and evaluated within a voltage range of 3.0 - 4.4 V at various current density (1 C = 200 mA g^{-1}).

1.7 ***Computational methods:***

In this work, the CP2K program was employed to optimize the system at the level of the PBE functional with DZVP-MOLOPT-SR-GTH basis sets and D3 dispersion correction. A cutoff energy of 400 eV was used to define the auxiliary plane-wave grid for the electronic density. To ensure the accuracy of the computed energies, the self-consistent field (SCF) procedure was considered converged when the total energy change between iterations was below 10^{-6}. In addition, the migration pathway and the corresponding energy variation of Li^+ within the crystal lattice were investigated using the climbing-image nudged elastic band (CI-NEB) method, allowing the minimum energy pathway and migration energy barriers to be determined. All visualizations were performed using VESTA.

The lithium electrodeposition behavior was simulated using the finite element method implemented in COMSOL Multiphysics 6.2. The simulation employed the tertiary current distribution and the deformed geometry module. The corresponding governing equations used for the calculations are summarized as follows. In the polymer electrolyte (PE), lithium migration is governed by the Nernst-Planck equation:

$$N_{Li+} = -D_{Li+}\left(\nabla c_0 - \frac{zFc_0}{RT}\nabla\Phi\right)$$

Where, N_{Li+} is the lithium flux, D_{Li+} is the lithium diffusion coefficient, z is the charge of lithium, c_0 is the concentration of lithium, F represents the Faraday constant, R is the ideal gas constant, T denotes the temperature in Kelvin, and Φ corresponds to the electrolyte potential. Lithium in the electrolyte follows the mass conservation and charge conservation equations. Where, c_i represents the concentration, and z_i is the valence of each substance in the PE.

$$\frac{\partial c_{Li+}}{\partial t} + \nabla \times N_{Li+} = 0$$

$$z_i c_i = 0$$

The electroplating of Li^+ at the electrolyte-negative electrode interface can be described by the following simplified reaction equation:

$$i = i_0\left[exp\left(\frac{\alpha_a F\eta}{RT}\right) - \frac{c_{Li^+}}{c_0} exp\left(\frac{\alpha_c F\eta}{RT}\right)\right]$$

Where, i_0 is the exchange current density, η is the overpotential, α_a and α_c are the anodic and cathodic charge transfer coefficients, respectively, and c_{Li^+} is the lithium concentration near the interface.

To study the initiation and propagation of lithium dendrites under realistic interface conditions, we strategically introduced four defects at the center of the model region (4 ×6 nm). These designed defects simulate local perturbations in surface energy and ion flux distribution, effectively replicating the inherent heterogeneity of actual lithium metal anodes (such as surface roughness, compositional variations, and interfacial instability). This deliberate introduction of initial defects can accelerate morphological evolution while maintaining physical relevance, thereby more accurately reflecting the growth kinetics of dendrites in operating battery systems.

2. Supporting Figures

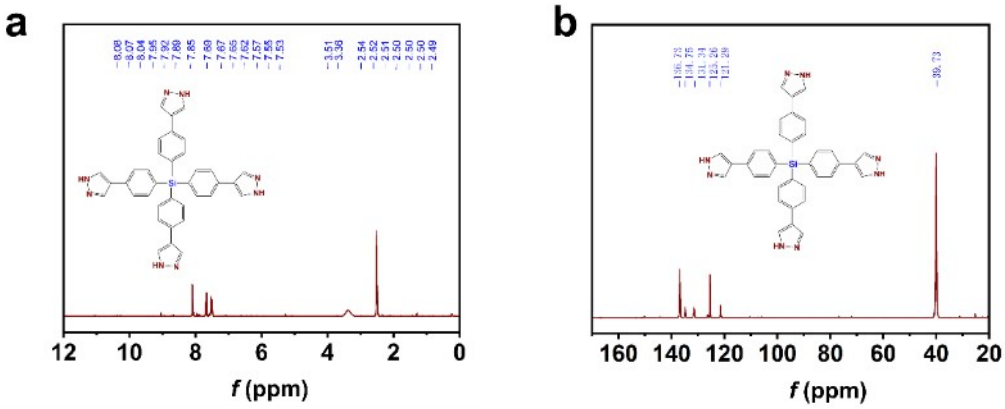

Figure S1 (a) ^{1}H-NMR spectra of TPPSi; (b) ^{13}C-NMR spectra of TPPSi.

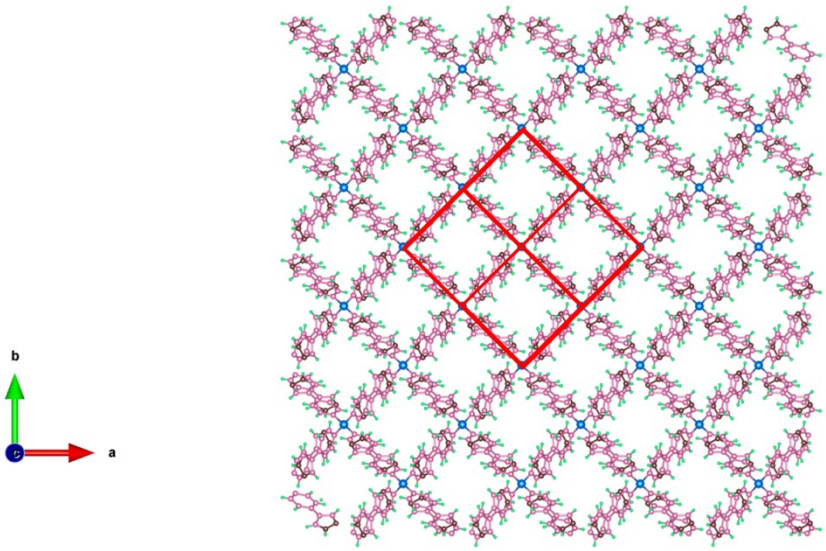

Figure S2 Schematic of crystalline Si-HOF.

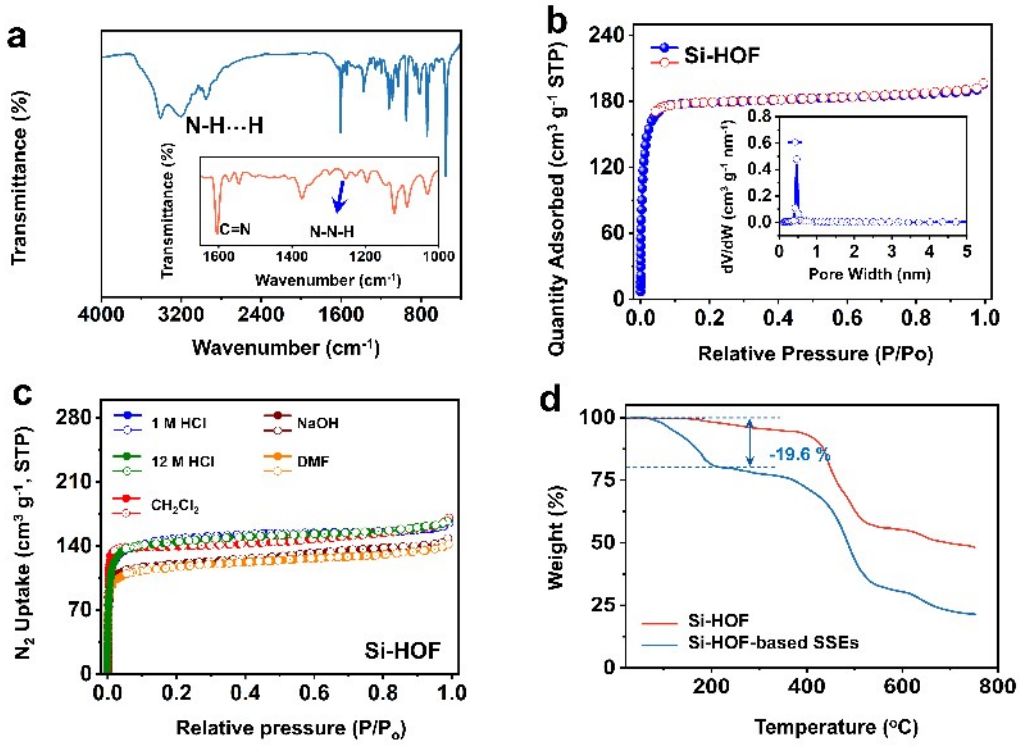

Figure S3 (a) FT-IR spectra of Si-HOF; (b) N_2 adsorption isotherm at 77 K of Si-HOF; (c) N_2 adsorption isotherm at 77 K of Si-HOF after immerse in various solution; (d) TGA curves.

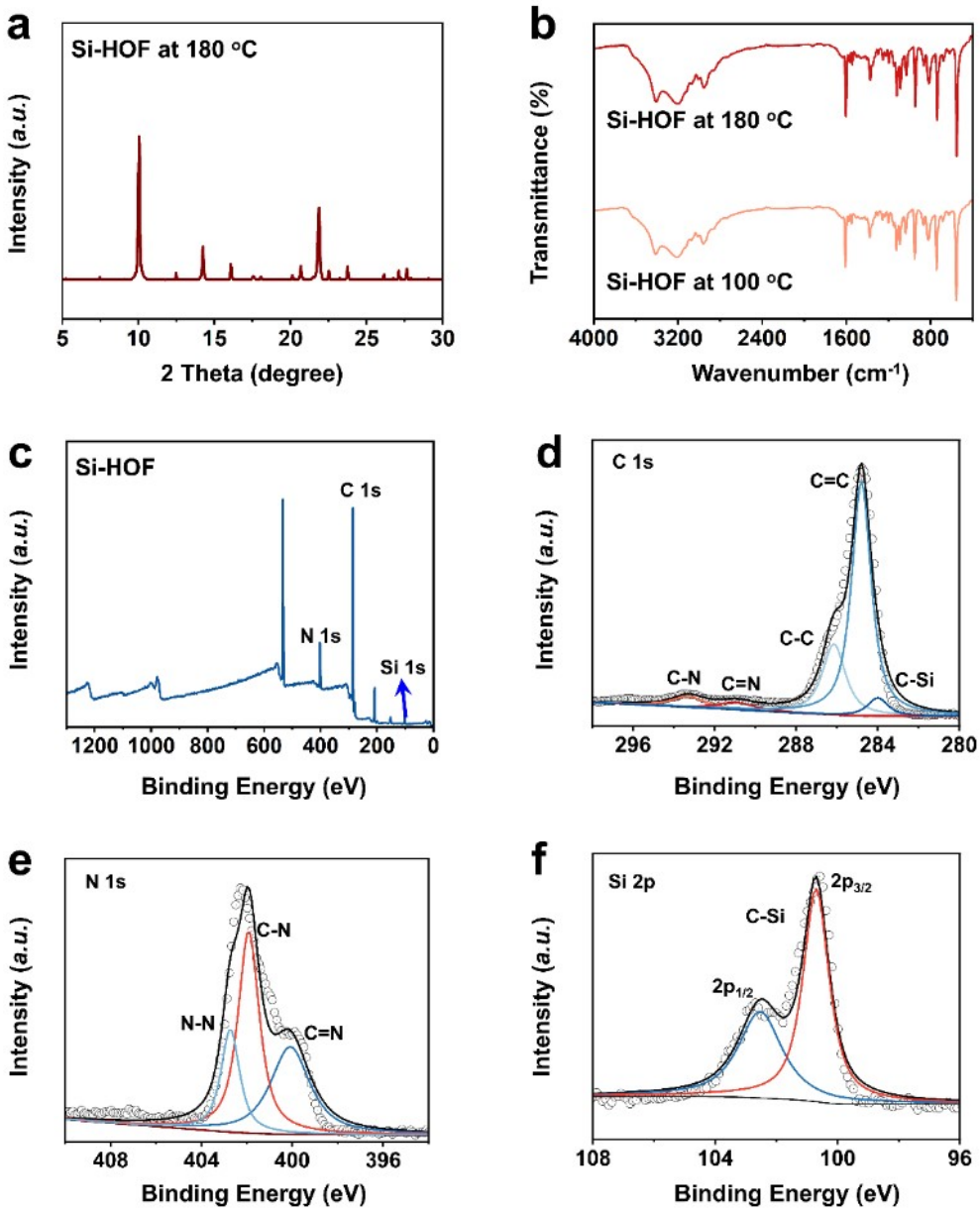

Figure S4 (a) XRD patterns of Si-HOF after heated to 180 °C; (b) FT-IR spectra of Si-HOF after heated to 100 °C and 180 °C; (c) XPS spectra of C Si-HOF; XPS spectra of C 1s (d), N 1s (e), Si 2p (f). The high-resolution C 1s spectrum can be deconvoluted into five components centered at 284.0, 284.8, 286.2, 290.9, and 286.3 eV, corresponding to C-Si, C=C/C-C, C=N, and C-N, respectively. The N 1s spectrum shows three peaks at 400.1, 401.8 and 402.7 eV, assigned to C=N, C-N and N-N, respectively, confirming the presence of the =N-NH- linkage and its involvement in hydrogen bonding. The high-resolution Si 2p spectrum exhibits a dominant doublet centered at 100.7 eV (Si 2p3/2), characteristic of Si-C bonds. A weak shoulder at higher binding energy (102.5 eV) can be attributed to minor surface oxidation, which is commonly observed due to air exposure.

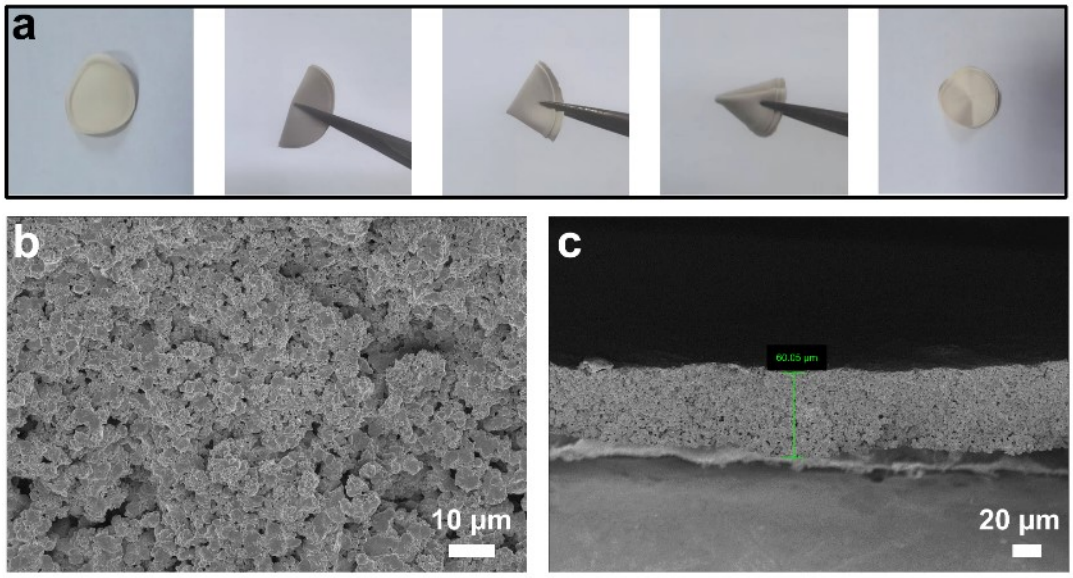

Figure S5 (a) Photograph of the Si-HOF-based SSEs; (b-c) SEM image of the cross-section of the Si-HOF-based SSEs.

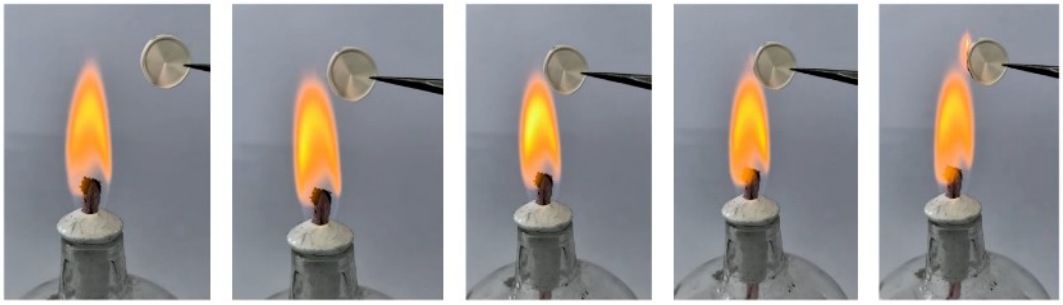

Figure S6 Flame test of the Si-HOF-based SSEs.

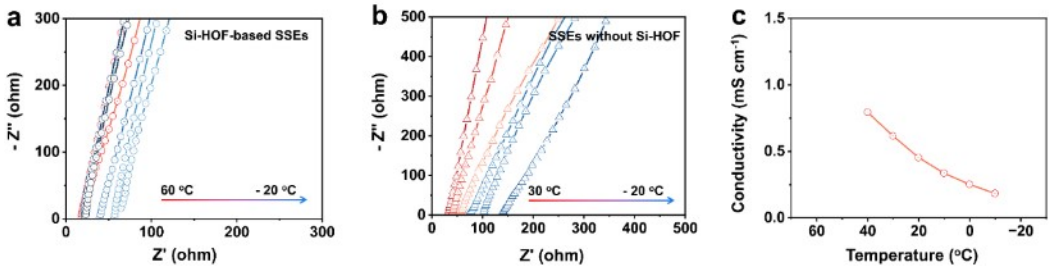

Figure S7 (a) EIS plot of Si-HOF-based SSEs at various temperature; (b) EIS plot of SSEs without Si-HOF at various temperature; (c) Ionic conductivities.

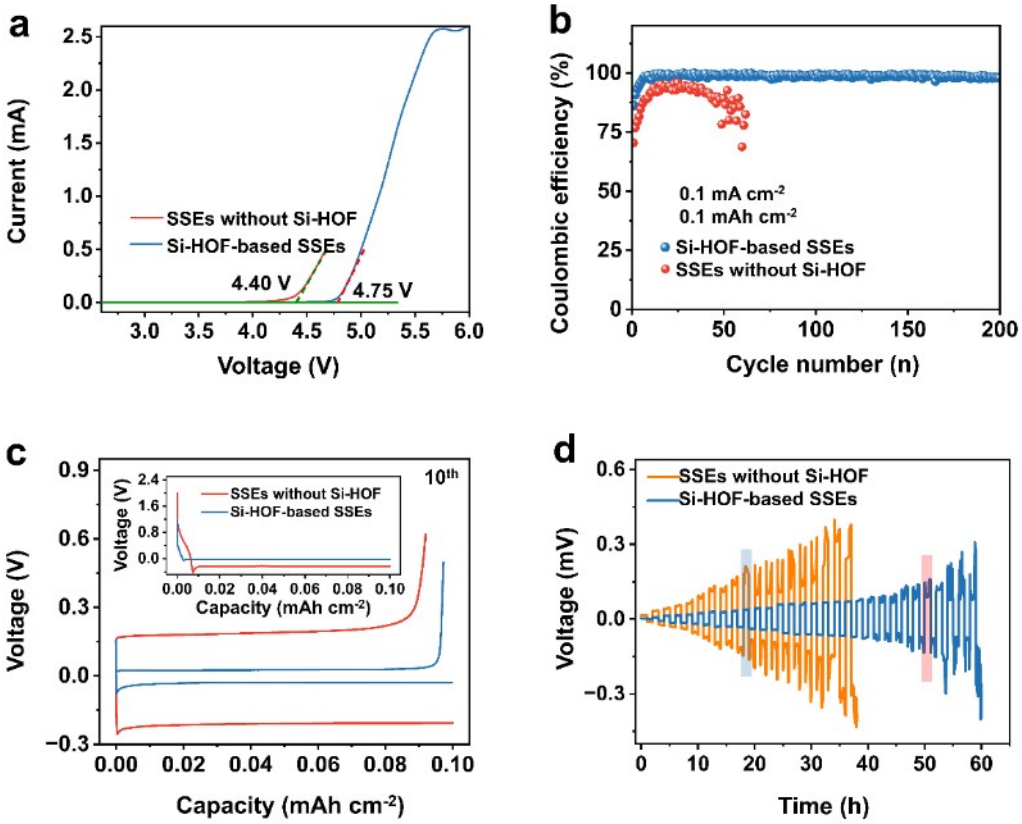

Figure S8 (a) Electrochemical stability window of Li|SSEs|SS battery; (b) Coulombic efficiency; (c) Comparisons of Li nucleation and voltage hysteresis; (d) CCD of the symmetric cells.

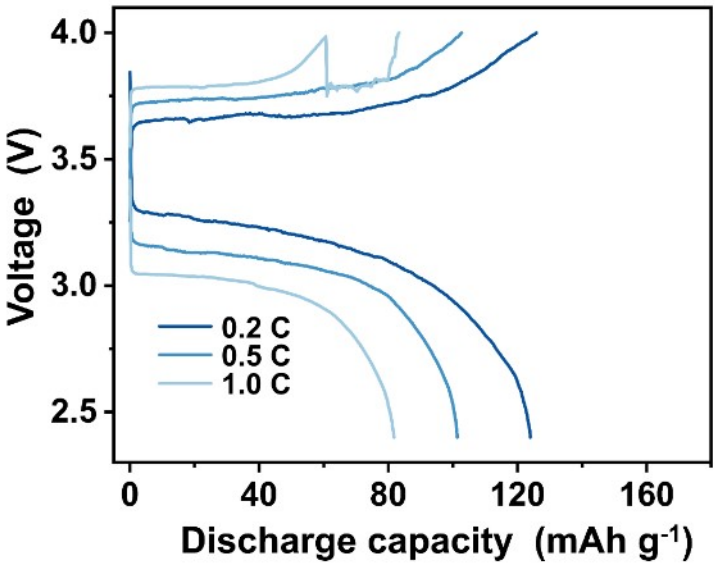

Figure S9 Charge and discharge curves of Li| SSEs without Si-HOF|LFP LMB.

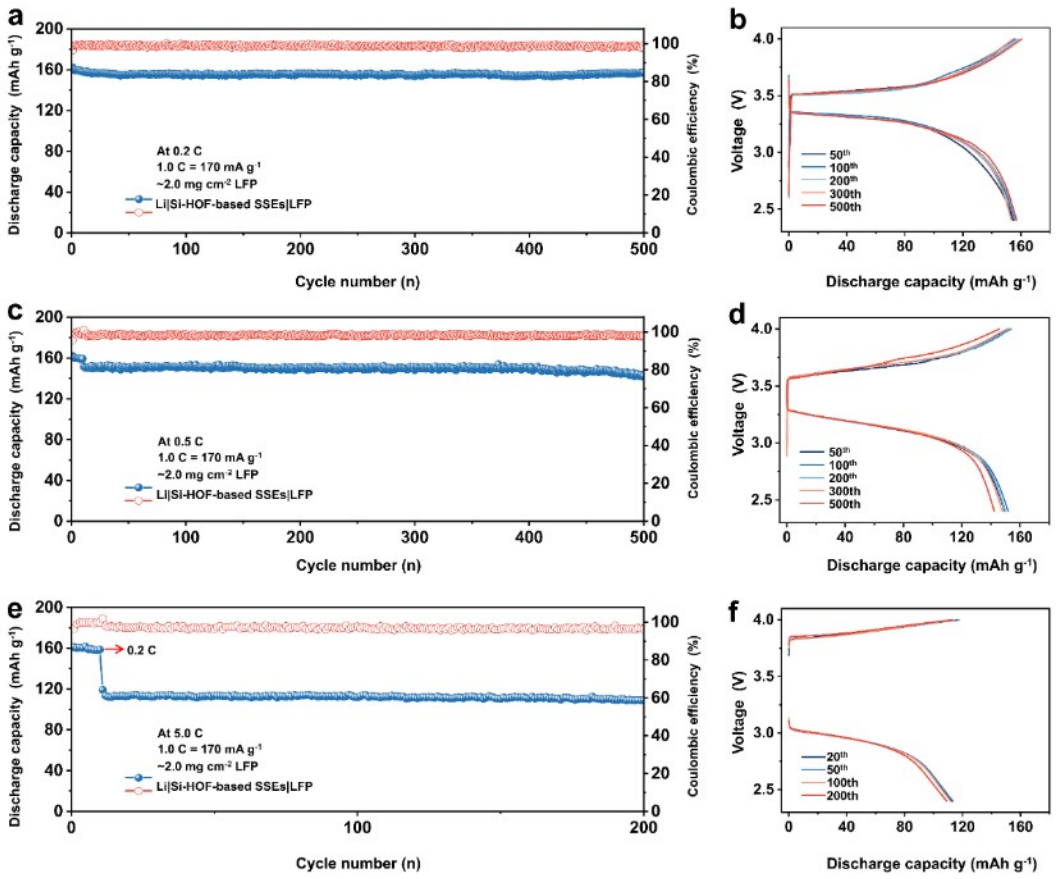

Figure S10 (a) Cycling in Li|Si-HOF-based SSEs|LFP LMB at 0.2 C; (b) Corresponding charge/discharge curves; (c) Cycling in Li|Si-HOF-based SSEs|LFP LMB at 0.5 C; (d) Corresponding charge/discharge curves; (e) Cycling in Li|Si-HOF-based SSEs|LFP LMB at 5.0 C; (f) Corresponding charge/discharge curves.

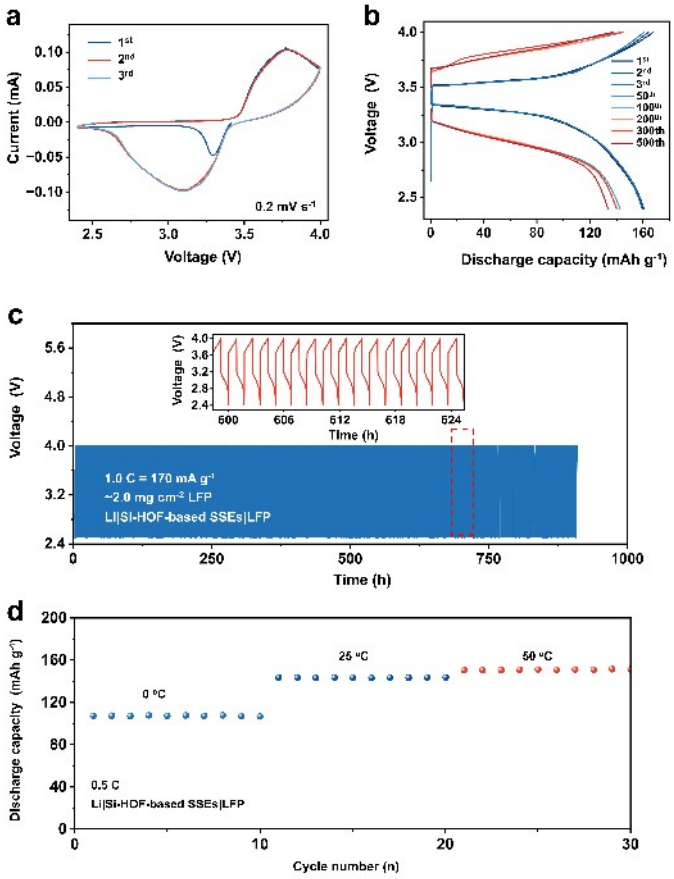

Figure S11 (a) CV curves of Li|Si-HOF-based SSEs|LFP LMB at 0.2 mV s^{-1}; (b) Corresponding charge/discharge curves; (c) Galvanostatic cycling of Li|Si-HOF-based SSEs|LFP; (d) Discharge specific capacity of the Li|Si-HOF SSEs|LFP LMB with Si-HOF-based SSEs at different temperatures.

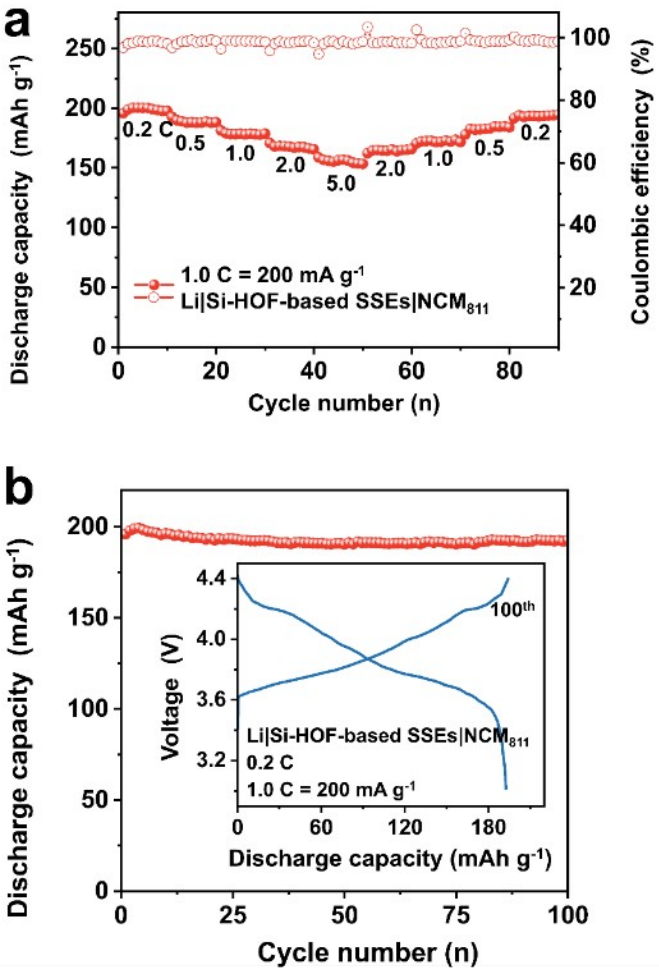

Figure S12 (a) Rate performance of the Li|Si-HOF-based SSEs|NCM_{811} LMB; (b) Cycling in Li|Si-HOF-based SSEs|NCM_{811} LMB at 0.2 C.

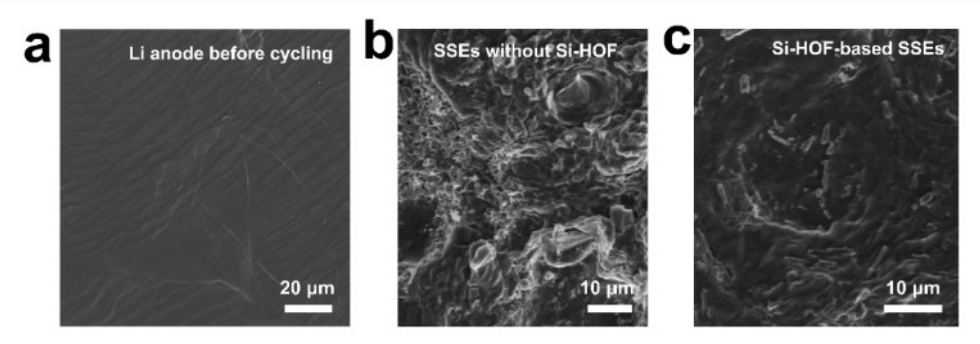

Figure S13 (a) SEM images of the lithium metal surface; SEM images of the lithium metal surface after Li plating/stripping in symmetric battery (b) without and (c) with Si-HOF.

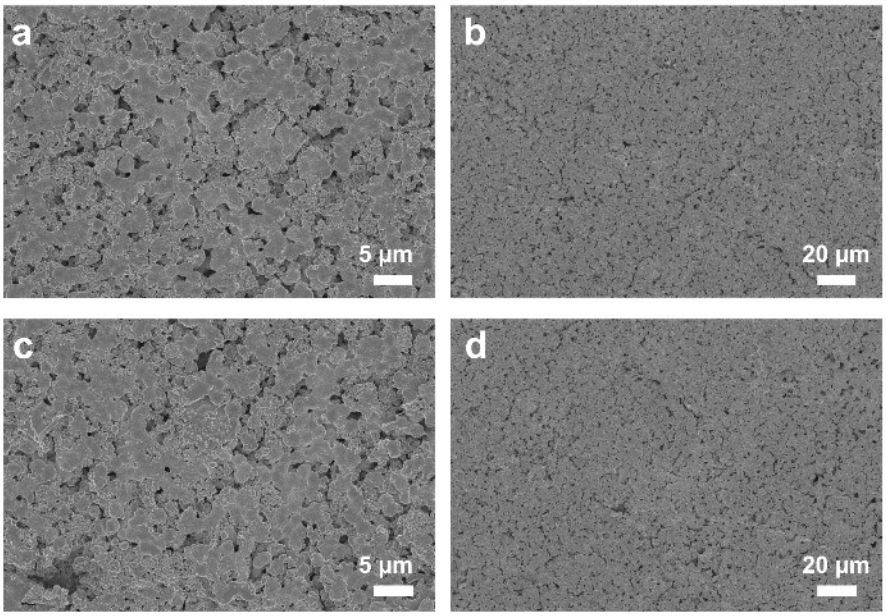

Figure S14 (a-d) SEM images of the surface of the Si-HOF-based SSEs after cycles.

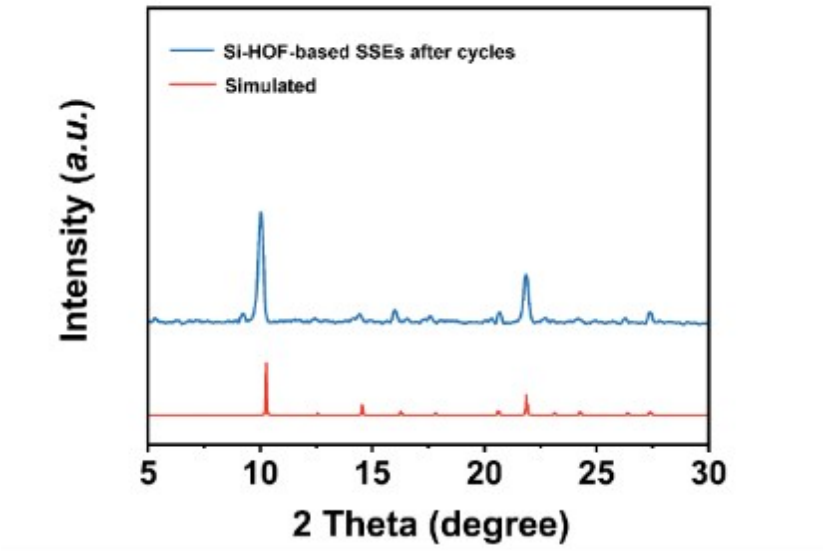

Figure S15 XRD patterns of Si-HOF-based SSEs after cycles.

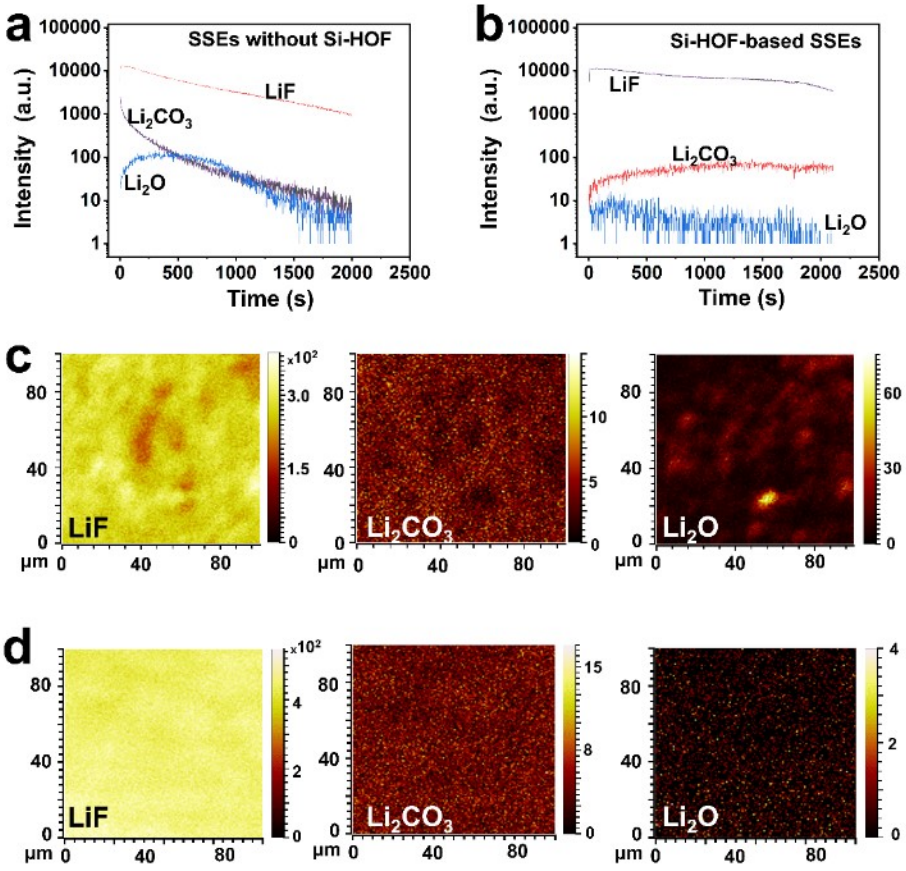

Figure S16 TOF-SIMS 2D (a-b) and 3D (c-d) spectra of LiF, Li_2CO_3 and Li_2O for SEI in Li anode surface in Li|Si-HOF-based SSEs|Li battery.

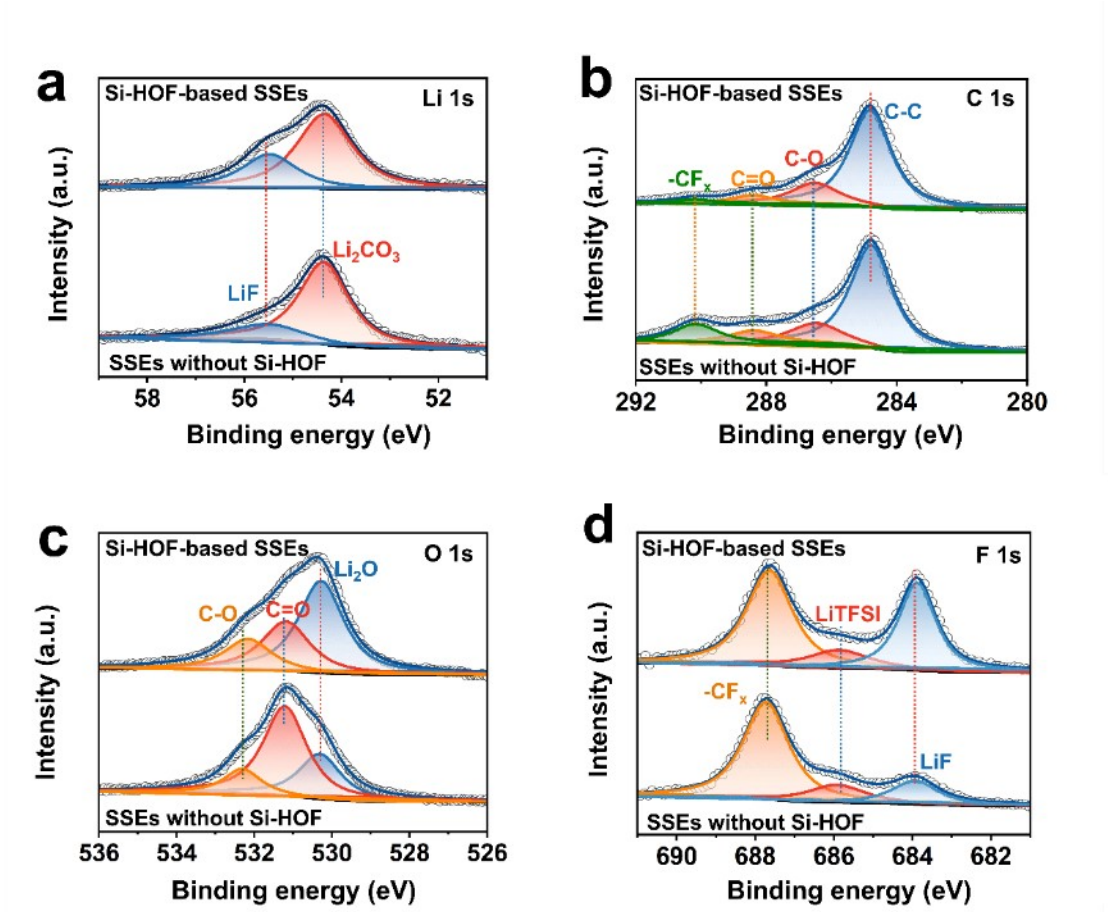

Figure S17 XPS spectra analysis of the SEI with or without Si-HOF: (a) Li 1s, (b) C 1s, (c) O 1s, (d) F 1s.

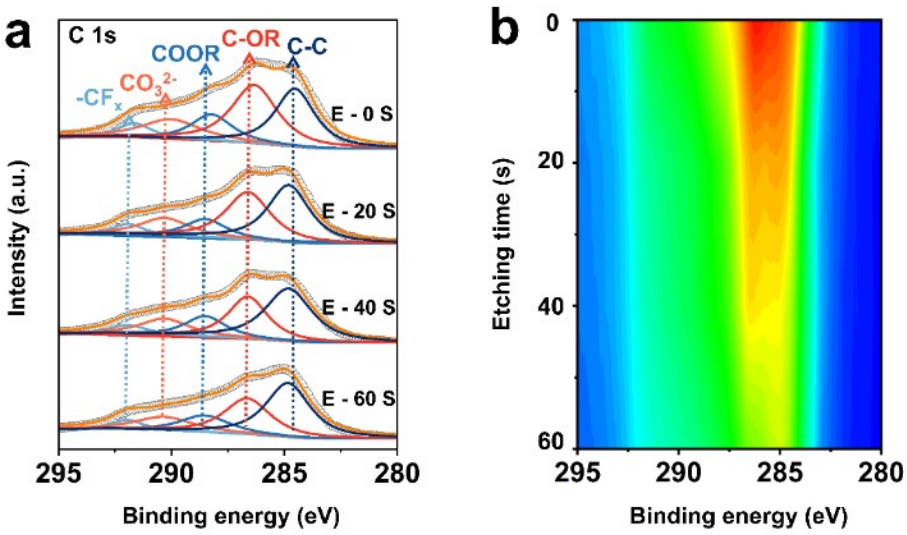

Figure S18 (a)-(b) C 1s spectra of Li anode after 100 cycles.

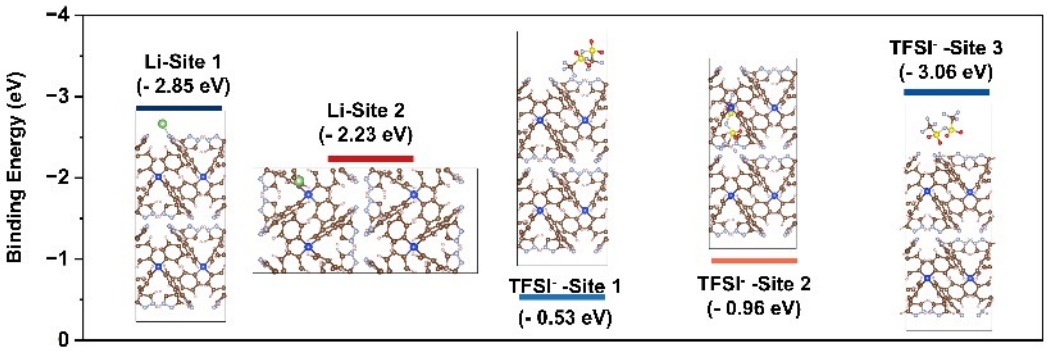

Figure S19 The simulated absorption energy between Si-HOF and LiTFSI.